Symmetry energy studies at intermediate energies: first experiment with the INDRA-FAZIA apparatus

Caterina Ciampi
GANIL

for the INDRA-FAZIA collaboration

22nd Zimányi School
Winter workshop on heavy ion physics

5-9 December 2022

Heavy ion collisions

The Fermi energy regime

Heavy ion collisions allow to study the properties of nuclei far from equilibrium conditions

→ different outcomes depending on **energy regime** and **reaction centrality**

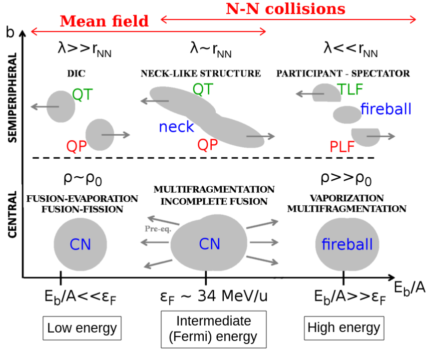

Heavy ion collisions

The Fermi energy regime

Heavy ion collisions allow to study the properties of nuclei far from equilibrium conditions

→ different outcomes depending on **energy regime** and **reaction centrality**

Intermediate energy regime

$20\,A\text{MeV} < E_b < 100\,A\text{MeV}$

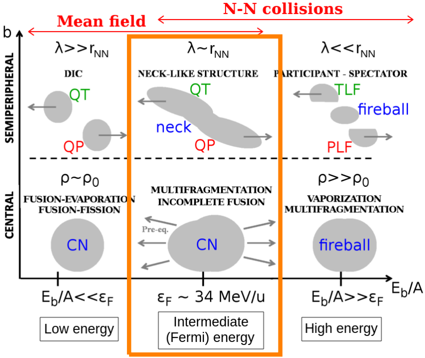

Heavy ion collisions

The Fermi energy regime

Heavy ion collisions allow to study the properties of nuclei far from equilibrium conditions

→ different outcomes depending on **energy regime** and **reaction centrality**

Intermediate energy regime

$20\,AMeV < E_b < 100\,AMeV$

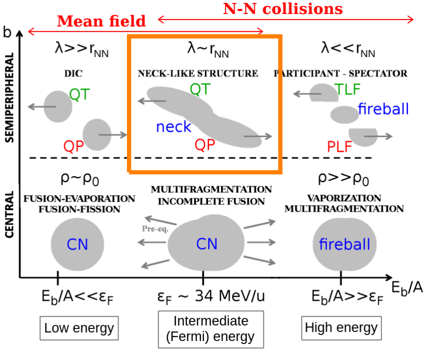

For **semiperipheral and peripheral** collisions:

- **Binary exit channel**: production of excited QP and QT (keeping memory of their initial identity), that then undergo statistical de-excitation

Heavy ion collisions

The Fermi energy regime

Heavy ion collisions allow to study the properties of nuclei far from equilibrium conditions

→ different outcomes depending on **energy regime** and **reaction centrality**

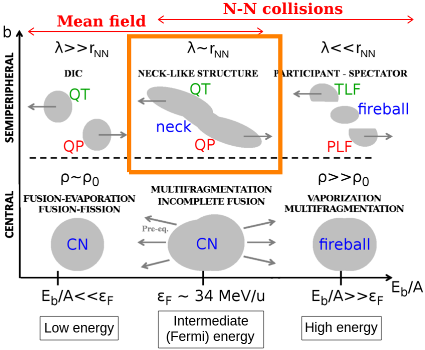

Intermediate energy regime
$20\,AMeV < E_b < 100\,AMeV$

For **semiperipheral and peripheral** collisions:

- **Binary exit channel**: production of excited QP and QT (keeping memory of their initial identity), that then undergo statistical de-excitation
- Deformed transient systems during projectile-target interaction
  - Contact phase: moderate compression of projectile and target

Heavy ion collisions

The Fermi energy regime

Heavy ion collisions allow to study the properties of nuclei far from equilibrium conditions

→ different outcomes depending on **energy regime** and **reaction centrality**

Intermediate energy regime
$20\,AMeV < E_b < 100\,AMeV$

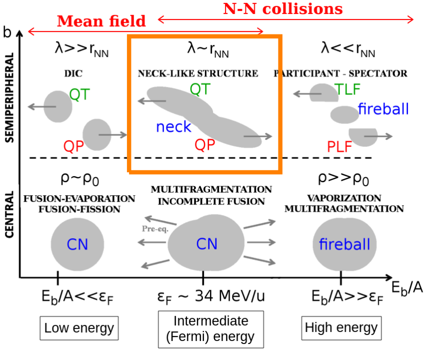

For **semiperipheral and peripheral** collisions:

- **Binary exit channel**: production of excited QP and QT (keeping memory of their initial identity), that then undergo statistical de-excitation
- Deformed transient systems during projectile-target interaction
  - Contact phase: moderate compression of projectile and target
  - Separation phase (late stage of contact phase): elongated low density *neck region* connects QP and QT ⇒ *midvelocity emission*

Heavy ion collisions at intermediate energies → collect information on the **Nuclear Equation of State**: energy per nucleon as a function of *density* $\rho = \rho_n + \rho_p$ and *isospin asymmetry* $\delta = \frac{\rho_n - \rho_p}{\rho_n + \rho_p}$. By defining $x = \left(\frac{\rho - \rho_0}{3\rho_0}\right)$:

$$\frac{E}{A}(\rho, \delta) = \frac{E}{A}(\rho) + \frac{E_{sym}}{A}(\rho)\delta^2 \quad \text{where} \quad \frac{E_{sym}}{A}(\rho) = E_{sym} + L_{sym}x + \frac{1}{2}K_{sym}x^2 + \ldots$$

Physics case

Nuclear Equation of State (NEoS) and isospin transport phenomena

Heavy ion collisions at intermediate energies → collect information on the **Nuclear Equation of State**: energy per nucleon as a function of *density* $\rho = \rho_n + \rho_p$ and *isospin asymmetry* $\delta = \frac{\rho_n - \rho_p}{\rho_n + \rho_p}$. By defining $x = \left(\frac{\rho - \rho_0}{3\rho_0}\right)$:

$$\frac{E}{A}(\rho, \delta) = \frac{E}{A}(\rho) + \frac{E_{sym}}{A}(\rho)\delta^2 \quad \text{where} \quad \frac{E_{sym}}{A}(\rho) = E_{sym} + L_{sym}x + \frac{1}{2}K_{sym}x^2 + \ldots$$

- The symmetry energy term governs the **isospin transport phenomena**:

$$\mathbf{j}_n - \mathbf{j}_p \propto \frac{E_{sym}}{A}(\rho)\nabla\delta + \delta\frac{\partial\frac{E_{sym}}{A}(\rho)}{\partial\rho}\nabla\rho$$

Physics case

Nuclear Equation of State (NEoS) and isospin transport phenomena

Heavy ion collisions at intermediate energies → collect information on the **Nuclear Equation of State**: energy per nucleon as a function of *density* $\rho = \rho_n + \rho_p$ and *isospin asymmetry* $\delta = \frac{\rho_n - \rho_p}{\rho_n + \rho_p}$. By defining $x = \left(\frac{\rho - \rho_0}{3\rho_0}\right)$:

$$\frac{E}{A}(\rho, \delta) = \frac{E}{A}(\rho) + \frac{E_{sym}}{A}(\rho)\delta^2 \quad \text{where} \quad \frac{E_{sym}}{A}(\rho) = E_{sym} + L_{sym}x + \frac{1}{2}K_{sym}x^2 + \dots$$

- The symmetry energy term governs the **isospin transport phenomena**:

$$\mathbf{j}_n - \mathbf{j}_p \propto \boxed{\frac{E_{sym}}{A}(\rho)\nabla\delta} + \delta\frac{\partial\frac{E_{sym}}{A}(\rho)}{\partial\rho}\nabla\rho$$

  - **Isospin diffusion**: driven by an isospin gradient in the system (e.g. asymmetric systems), leading to isospin equilibration. Sensitive to $E_{sym}(\rho)/A$

Physics case

Nuclear Equation of State (NEoS) and isospin transport phenomena

Heavy ion collisions at intermediate energies → collect information on the **Nuclear Equation of State**: energy per nucleon as a function of *density* $\rho = \rho_n + \rho_p$ and *isospin asymmetry* $\delta = \frac{\rho_n - \rho_p}{\rho_n + \rho_p}$. By defining $x = \left(\frac{\rho - \rho_0}{3\rho_0}\right)$:

$$\frac{E}{A}(\rho, \delta) = \frac{E}{A}(\rho) + \frac{E_{sym}}{A}(\rho)\delta^2 \quad \text{where} \quad \frac{E_{sym}}{A}(\rho) = E_{sym} + L_{sym}x + \frac{1}{2}K_{sym}x^2 + \ldots$$

- The symmetry energy term governs the **isospin transport phenomena**:

$$\mathbf{j}_n - \mathbf{j}_p \propto \frac{E_{sym}}{A}(\rho)\nabla\delta + \boxed{\delta \frac{\partial \frac{E_{sym}}{A}(\rho)}{\partial \rho} \nabla \rho}$$

  - **Isospin diffusion**: driven by an isospin gradient in the system (e.g. asymmetric systems), leading to isospin equilibration. Sensitive to $E_{sym}(\rho)/A$
  - **Isospin drift** (or *isospin migration*): driven by density gradient (e.g. neck $\rho \lesssim \rho_0$). Can be isolated by choosing a symmetric system. Sensitive to $\frac{\partial E_{sym}(\rho)/A}{\partial \rho}$

Breakup of the QP

Characteristics of the breakup channel

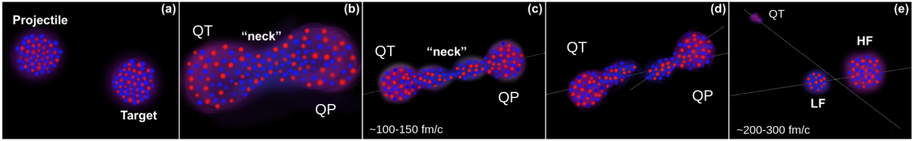

adapted from A. Rodriguez Manso et al., PRC 95, 044604 (2017)

Breakup or dynamical fission: **fast, asymmetric and anisotropic** fission process, with a time scale of $\sim 200 - 300\,\text{fm/c}$:

- Different from *statistical fission*, a de-excitation process taking place in longer time scales and characterised by isotropic angular distribution

Breakup of the QP

Characteristics of the breakup channel

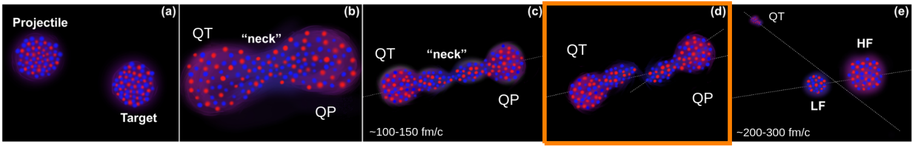

adapted from A. Rodriguez Manso et al., PRC 95, 044604 (2017)

Breakup or dynamical fission: **fast, asymmetric and anisotropic** fission process, with a time scale of $\sim 200 - 300\,\mathrm{fm/c}$:

- Different from *statistical fission*, a de-excitation process taking place in longer time scales and characterised by isotropic angular distribution
- A possible intepretation of the phenomenon:
  - QP, QT separate featuring a strong deformation + angular momentum

Breakup of the QP

Characteristics of the breakup channel

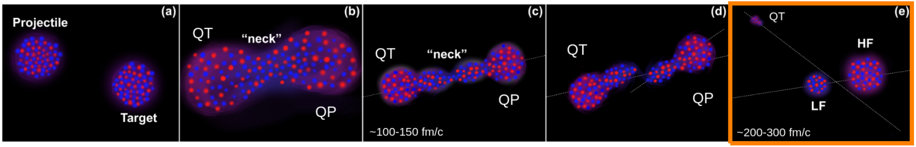

adapted from A. Rodriguez Manso et al., PRC 95, 044604 (2017)

Breakup or dynamical fission: **fast, asymmetric and anisotropic** fission process, with a time scale of $\sim 200 - 300\,\mathrm{fm/c}$:

- Different from *statistical fission*, a de-excitation process taking place in longer time scales and characterised by isotropic angular distribution
- A possible intepretation of the phenomenon:
  - QP, QT separate featuring a strong deformation + angular momentum
  - Prompt breakup → formation of a Light Fragment (LF, from the neck side) and a Heavy Fragment (HF) → **asymmetric**

Breakup of the QP

Characteristics of the breakup channel

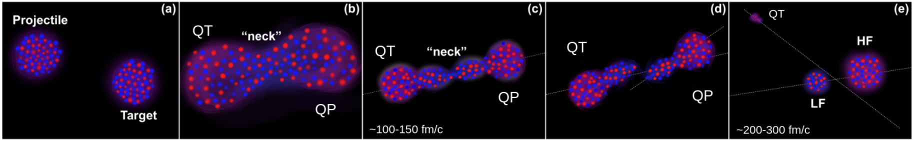

adapted from A. Rodriguez Manso et al., PRC 95, 044604 (2017)

Breakup or dynamical fission: **fast, asymmetric and anisotropic** fission process, with a time scale of $\sim 200 - 300\,\mathrm{fm/c}$:

- Different from *statistical fission*, a de-excitation process taking place in longer time scales and characterised by isotropic angular distribution
- A possible intepretation of the phenomenon:
  - QP, QT separate featuring a strong deformation + angular momentum
  - Prompt breakup $\rightarrow$ formation of a Light Fragment (LF, from the neck side) and a Heavy Fragment (HF) $\rightarrow$ **asymmetric**
  - **Fast** process $\rightarrow$ LF emitted towards CM $\rightarrow$ **anisotropic**

Breakup of the QP

Characteristics of the breakup channel

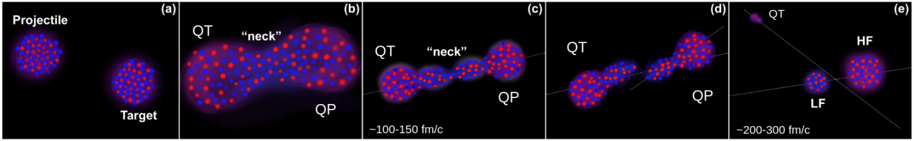

adapted from A. Rodriguez Manso et al., PRC 95, 044604 (2017)

Breakup or dynamical fission: **fast, asymmetric and anisotropic** fission process, with a time scale of $\sim 200 - 300\,\text{fm/c}$:

- Different from *statistical fission*, a de-excitation process taking place in longer time scales and characterised by isotropic angular distribution
- A possible intepretation of the phenomenon:
  - QP, QT separate featuring a strong deformation + angular momentum
  - Prompt breakup → formation of a Light Fragment (LF, from the neck side) and a Heavy Fragment (HF) → **asymmetric**
  - **Fast** process → LF emitted towards CM → **anisotropic**
- Isospin equilibration also between the two breakup fragments

What do we need?

What do we need?

The experimental requirements

Isotopic identification (Z, A)

Mandatory to build isospin related observables for:

- QP remnant
- QP breakup fragments
- light ejectiles from QP decay

What do we need?

The experimental requirements

Isotopic identification (Z, A)

Mandatory to build isospin related observables for:

- QP remnant
- QP breakup fragments
- light ejectiles from QP decay

Large angular coverage

Provides a good reconstruction of the global event:

- build global observables for centrality estimation
- investigate different emitting sources

What do we need?

The experimental requirements

Isotopic identification (Z, A)

Mandatory to build isospin related observables for:

- QP remnant
- QP breakup fragments
- light ejectiles from QP decay

Large angular coverage

Provides a good reconstruction of the global event:

- build global observables for centrality estimation
- investigate different emitting sources

The INDRA-FAZIA apparatus aims to overcome the most common limitations and to collect the most comprehensive information on the event.

INDRA and FAZIA are both multi-detector apparatuses, designed for the detection of charged fragments produced in heavy ion collisions at Fermi energies.

Experimental setup
INDRA

INDRA *(Identification de Noyaux et Détection avec Résolutions Accrues)*: highly segmented array for detection and identification of charged products of heavy ion collisions at intermediate energies ($10 < E < 100\,A$MeV).

- Original configuration of 17 rings:
  - 1: Si + CsI(Tl)
  - 2-9: Ionisation ch. + Si + CsI(Tl)
  - 10-17: Ionisation ch. + CsI(Tl)
- Charge discrimination up to uranium, mass discrimination up to $Z = 4 - 5$, with low thresholds
- Large solid angle coverage (90%)
- High granularity (336 modules) → large particle multiplicity ($M_{tot}^{max} \sim 50$)

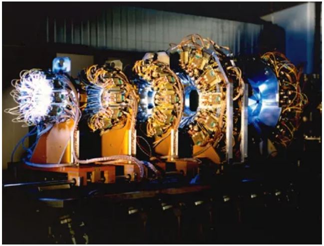

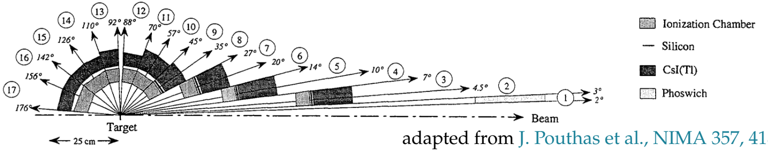

adapted from J. Pouthas et al., NIMA 357, 418 (1995)

INDRA *(Identification de Noyaux et Détection avec Résolutions Accrues)*: highly segmented array for detection and identification of charged products of heavy ion collisions at intermediate energies ($10 < E < 100\,A$MeV).

- Original configuration of 17 rings:
  - 1: Si + CsI(Tl)
  - 2-9: ~~Ionisation ch.~~ + Si + CsI(Tl)
  - 10-17: ~~Ionisation ch.~~ + CsI(Tl)
- Charge discrimination up to uranium, mass discrimination up to $Z = 4-5$, with low thresholds
- Large solid angle coverage (90%)

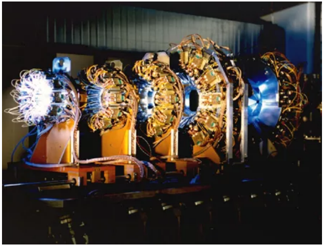

- High granularity (336 modules) → large particle multiplicity ($M_{tot}^{max} \sim 50$)

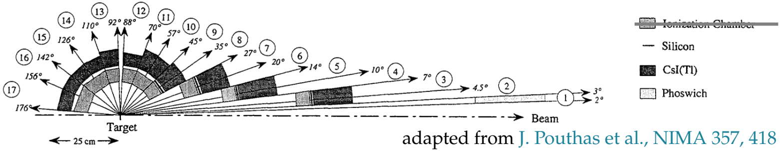

adapted from J. Pouthas et al., NIMA 357, 418 (1995)

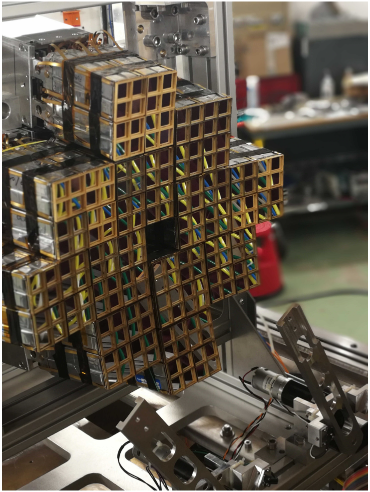

FAZIA *(Forward-angle A and Z Identification Array)*: state of the art of ion identification in the Fermi energy domain.

- Result of R&D activities to refine:
  - detector performance
  - digital treatment of signals

Experimental setup
FAZIA

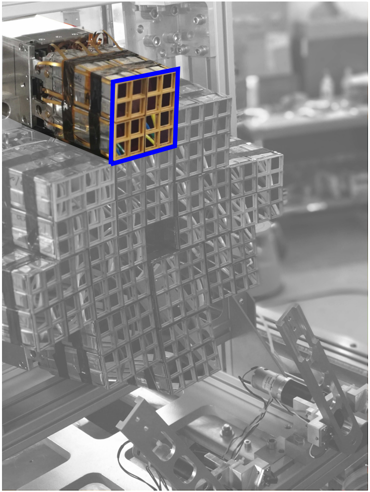

FAZIA *(Forward-angle A and Z Identification Array)*: state of the art of ion identification in the Fermi energy domain.

- Result of R&D activities to refine:
  - detector performance
  - digital treatment of signals
- Basic module: **block**, consisting of 16 three stage **telescopes** ($2 \times 2\,\text{cm}^2$ active area):
  - Si1 300 μm thick
  - Si2 500 μm thick
  - CsI(Tl) 10cm thick

Experimental setup
FAZIA

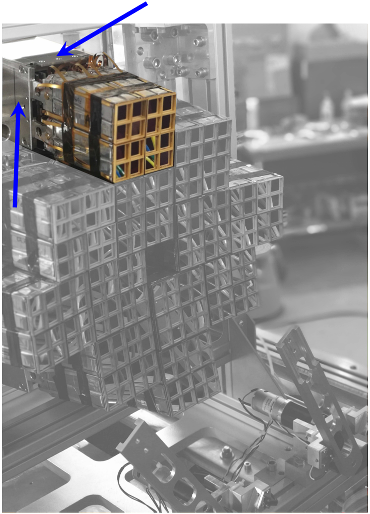

FAZIA *(Forward-angle A and Z Identification Array)*: state of the art of ion identification in the Fermi energy domain.

- Result of R&D activities to refine:
  - detector performance
  - digital treatment of signals
- Basic module: **block**, consisting of 16 three stage **telescopes** ($2 \times 2\,\mathrm{cm}^2$ active area):
  - Si1 300 μm thick
  - Si2 500 μm thick
  - CsI(Tl) 10cm thick

  Each block is equipped with the read-out electronics for all of its telescopes.

Experimental setup

FAZIA

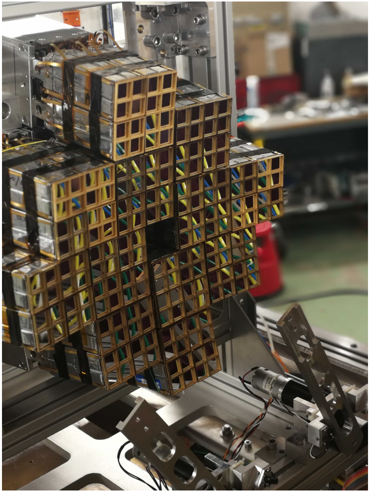

FAZIA *(Forward-angle A and Z Identification Array)*: state of the art of ion identification in the Fermi energy domain.

- Result of R&D activities to refine:
  - detector performance
  - digital treatment of signals
- Basic module: **block**, consisting of 16 three stage **telescopes** ($2 \times 2\,\mathrm{cm}^2$ active area):
  - Si1 300 μm thick
  - Si2 500 μm thick
  - CsI(Tl) 10cm thick

  Each block is equipped with the read-out electronics for all of its telescopes.
- Identification techniques: ΔE-E / PSA
  - Charge discrimination tested up to $Z \sim 55$
  - Mass discrimination up to $Z \sim 25$ / $Z \sim 22$

Experimental setup

The INDRA-FAZIA coupling

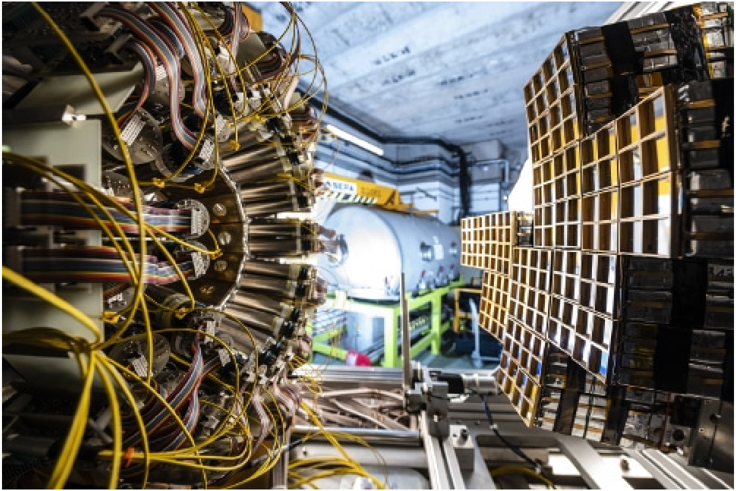

During the first months of 2019 the coupling between INDRA and FAZIA was completed in GANIL (Caen, FR).

Experimental setup

The INDRA-FAZIA coupling

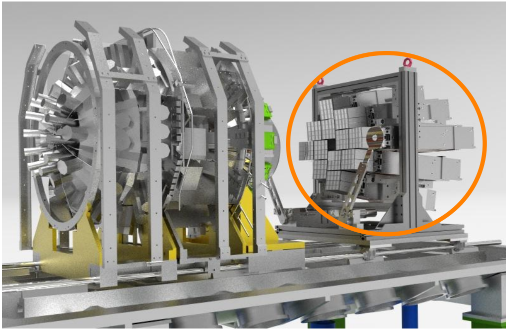

- The most forward polar angles (1.4°< θ< 12.6°) have been covered with 12 FAZIA blocks in a wall configuration at 1 m from the target. The first five rings of INDRA have been removed.
  $\rightarrow$ *isotopic identification of QP-like fragments*

Experimental setup

The INDRA-FAZIA coupling

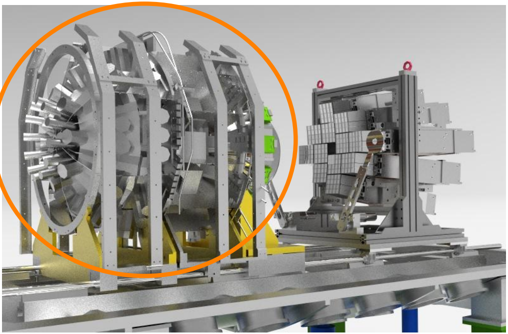

- The most forward polar angles (1.4°<θ< 12.6°) have been covered with 12 FAZIA blocks in a wall configuration at 1 m from the target. The first five rings of INDRA have been removed.
  $\longrightarrow$ *isotopic identification of QP-like fragments*
- The remaining part of INDRA (rings 6-17) covers the polar angles between 14° and 176° (~ 80% of the 4π solid angle).
  $\longrightarrow$ *global variables for the estimation of the reaction centrality*

The E789 experiment

New insights on the symmetry energy term of the Nuclear Equation of State

The E789 experiment (april-may 2019) is the first campaign to exploit the coupled INDRA-FAZIA apparatus:

- All of the four possible combinations of the two reaction partners ^{58}Ni and ^{64}Ni have been studied
  ⇒ compare the products of the two asymmetric reactions with those of both the neutron rich and neutron deficient symmetric systems
- Two different incident beam energies 32 AMeV and 52 AMeV
  ⇒ different timescale of the interaction process and different inspected nuclear density range

The E789 experiment

New insights on the symmetry energy term of the Nuclear Equation of State

The E789 experiment (april-may 2019) is the first campaign to exploit the coupled INDRA-FAZIA apparatus:

- All of the four possible combinations of the two reaction partners ^{58}Ni and ^{64}Ni have been studied
  $\Rightarrow$ compare the products of the two asymmetric reactions with those of both the neutron rich and neutron deficient symmetric systems
- Two different incident beam energies 32 AMeV and 52 AMeV
  $\Rightarrow$ different timescale of the interaction process and different inspected nuclear density range

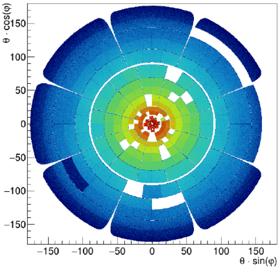

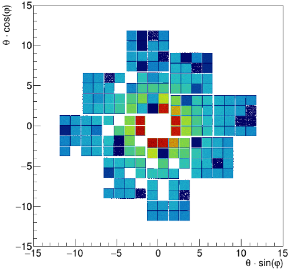

$\rightarrow$ Comparison of experimental results with AMD+GEMINI++ simulations, filtered according to the actual apparatus acceptance (mandatory to obtain information on physics processes)

QP evaporation channel (QPr)

QP evaporation channel

QPr channel selection

QP remnant: $\mathbf{M_{big} = 1}$, with $Z_{big} \geq 15$ and $\theta_{big}^{CM} < 90°$ ($v_z^{CM} > 0$)

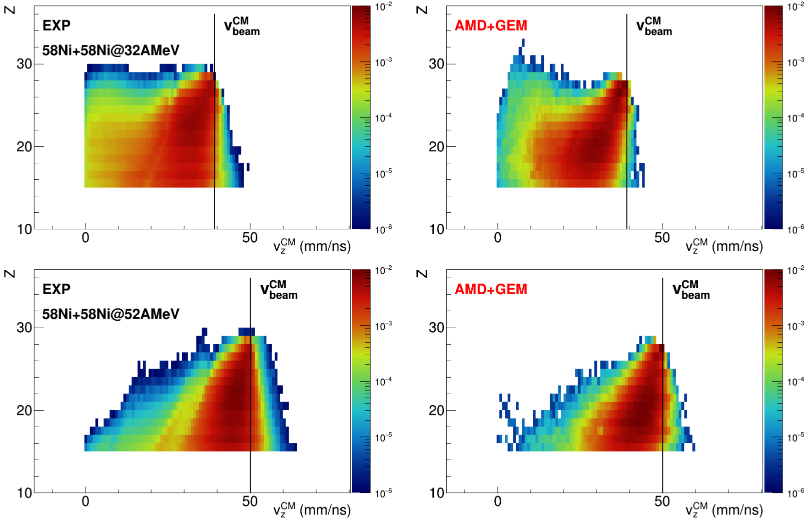

QP evaporation channel

QPr channel selection

QP remnant: $\mathbf{M_{big} = 1}$, with $Z_{big} \geq 15$ and $\theta^{CM}_{big} < 90°$ $(v^{CM}_z > 0)$

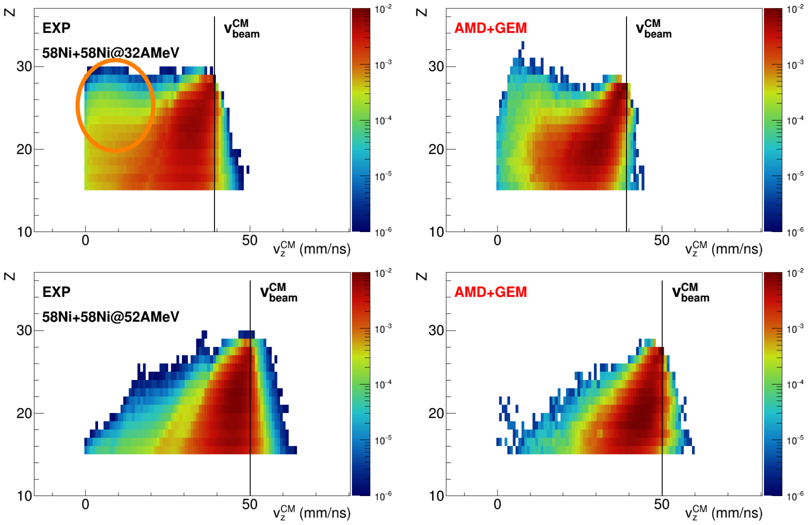

QP evaporation channel

QPr channel selection

QP remnant: $\mathbf{M_{big} = 1}$, with $Z_{big} \geq 15$ and $\theta_{big}^{CM} < 90°$ ($v_z^{CM} > 0$)

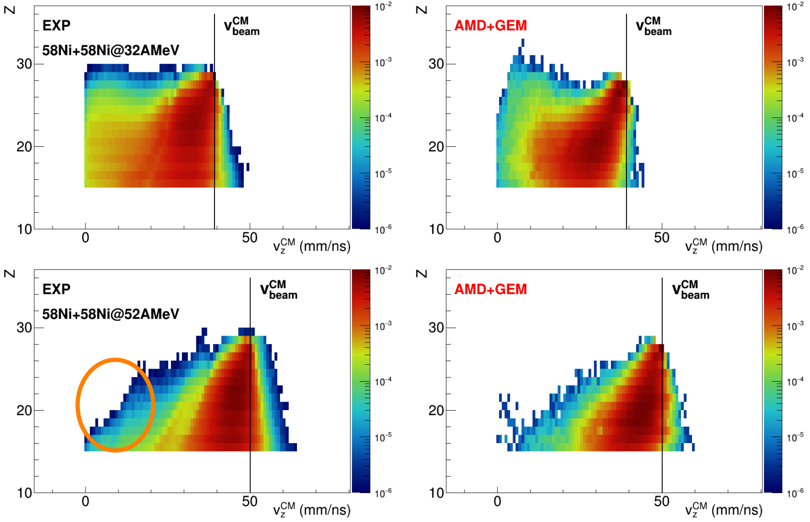

Reaction centrality estimation

Reduced QP momentum along the beam axis p_{red}

As reaction centrality estimator we select the **reduced momentum along the z-axis:**

$$p_{red} = \frac{p_z^{QP}}{p_{beam}}$$

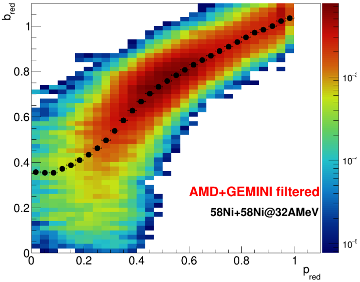

Reaction centrality estimation

Reduced QP momentum along the beam axis p_{red}

As reaction centrality estimator we select the **reduced momentum along the z-axis:**

$$p_{red} = \frac{p_z^{QP}}{p_{beam}}$$

Its correlation with $b_{red} = b/b_{gr}$ is:

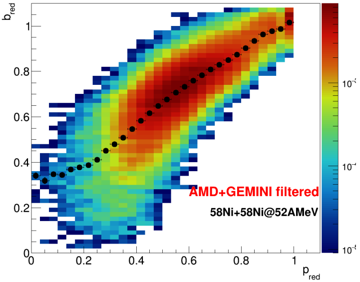

Reaction centrality estimation

Reduced QP momentum along the beam axis p_{red}

As reaction centrality estimator we select the **reduced momentum along the z-axis:**

$$p_{red} = \frac{p_z^{QP}}{p_{beam}}$$

Its correlation with $b_{red} = b/b_{gr}$ is:

- realiable for $p_{red} \gtrsim 0.3$

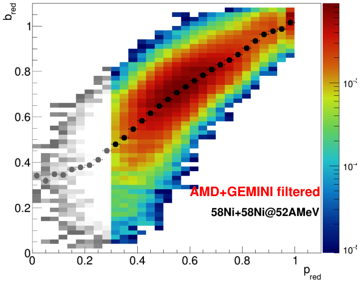

Reaction centrality estimation

Reduced QP momentum along the beam axis p_{red}

As reaction centrality estimator we select the **reduced momentum along the z-axis:**

$$p_{red} = \frac{p_z^{QP}}{p_{beam}}$$

Its correlation with $b_{red} = b/b_{gr}$ is:

- realiable for $p_{red} \gtrsim 0.3$
- the same for reactions at same energy

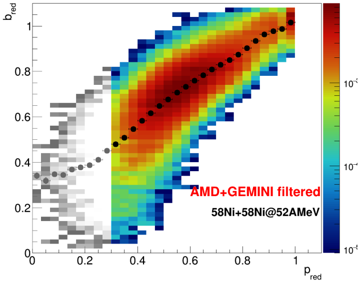

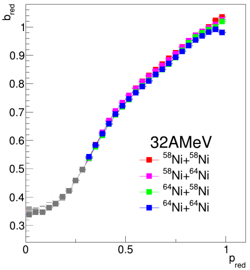

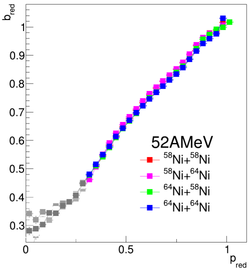

Reaction centrality estimation

Reduced QP momentum along the beam axis p_{red}

As reaction centrality estimator we select the **reduced momentum along the z-axis:**

$$p_{red} = \frac{p_z^{QP}}{p_{beam}}$$

Its correlation with $b_{red} = b/b_{gr}$ is:

- realiable for $p_{red} \gtrsim 0.3$
- the same for reactions at same energy
- similar for same system at two energies

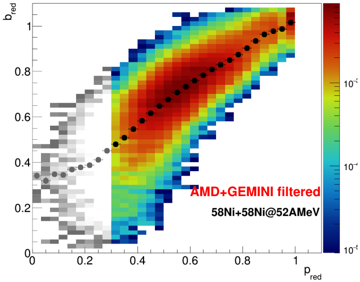

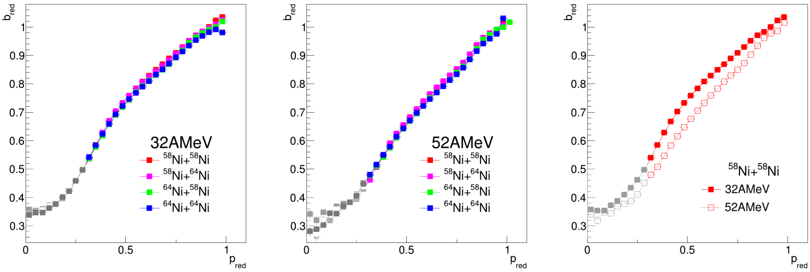

QP evaporation channel

Isospin diffusion: $\langle N/Z \rangle$ of the QP remnant

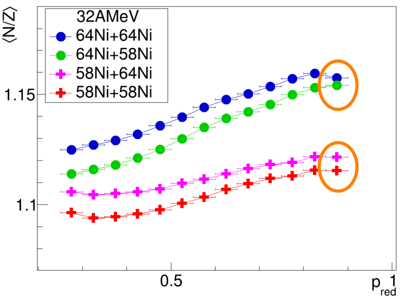

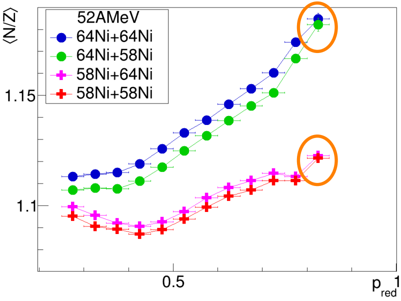

QP-QT equilibration in mixed systems:

- peripheral: similar $\langle N/Z \rangle$ for reactions induced by same projectile

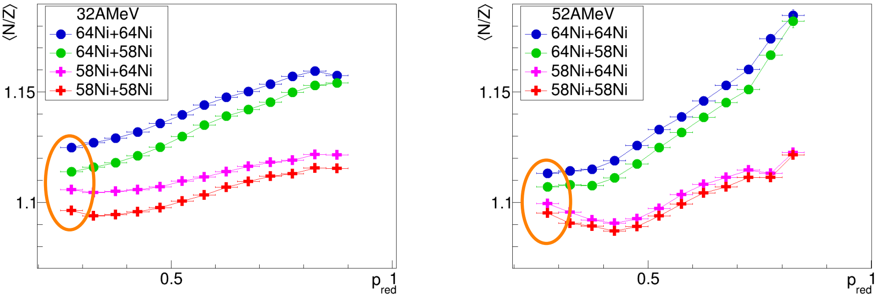

QP-QT equilibration in mixed systems:

- peripheral: similar $\langle N/Z \rangle$ for reactions induced by same projectile
- more central: $\langle N/Z \rangle$ depends on target

→ **evidence of isospin diffusion**, more clear at 32 AMeV

QP evaporation channel

Isospin diffusion: $\langle N/Z \rangle$ of the QP remnant

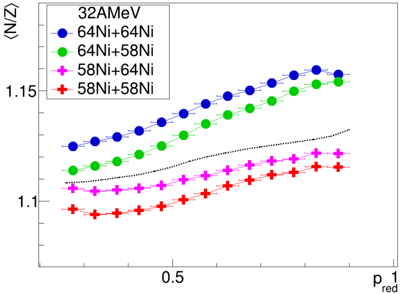

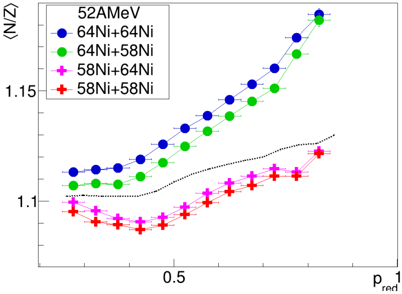

QP-QT equilibration in mixed systems:

- peripheral: similar $\langle N/Z \rangle$ for reactions induce
- more central: $\langle N/Z \rangle$ depends on target

$\rightarrow$ **evidence of isospin diffusion**, more clear at 32

Decreasing behaviour with centrality
$\rightarrow$ **Evaporation Attractor Line (EAL)**

$$A = 2.072\, Z + 2.32 \times 10^{-3} Z^2$$

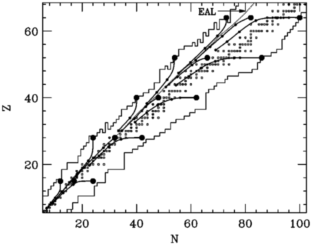

R. J. Charity, PRC58, 1073 (1998)

Isospin transport ratio technique: highlight isospin diff. F. Rami et al., PRL84, 1120 (2000)

Given $A = ^{64}$Ni, $B = ^{58}$Ni:

$$R(X) = \frac{2X_i - X_{AA} - X_{BB}}{X_{AA} - X_{BB}}$$

where $i = AA, AB, BA, BB$ and X is an isospin sensitive observable (e.g. $\langle N/Z \rangle_{QPr}$).
→ bypass effects acting similarly on the four systems (apparatus acceptance or physical processes e.g. statistical decay)

Isospin transport ratio technique: highlight isospin diff. F. Rami et al., PRL84, 1120 (2000)

Given $A = {}^{64}$Ni, $B = {}^{58}$Ni:

$$R(X) = \frac{2X_i - X_{AA} - X_{BB}}{X_{AA} - X_{BB}}$$

where $i = AA, AB, BA, BB$ and X is an isospin sensitive observable (e.g. $\langle N/Z \rangle_{QPr}$).
→ bypass effects acting similarly on the four systems (apparatus acceptance or physical processes e.g. statistical decay)

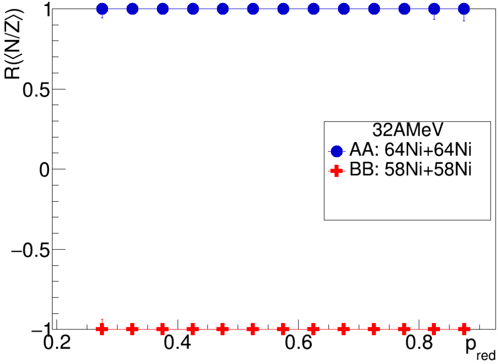

QP evaporation channel

Isospin diffusion: Isospin transport ratio

Isospin transport ratio technique: highlight isospin diff. F. Rami et al., PRL84, 1120 (2000)

Given $A = ^{64}$Ni, $B = ^{58}$Ni:

$$R(X) = \frac{2X_i - X_{AA} - X_{BB}}{X_{AA} - X_{BB}}$$

$\nearrow$ $R(X) = \pm 1 \rightarrow$ non equilibrated cond.

where $i = AA, AB, BA, BB$ and X is an isospin sensitive observable (e.g. $\langle N/Z \rangle_{QPr}$).

$\rightarrow$ bypass effects acting similarly on the four systems (apparatus acceptance or physical processes e.g. statistical decay)

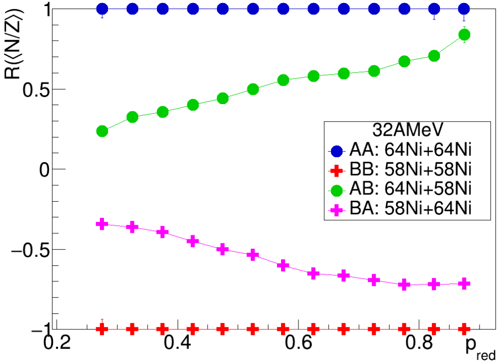

QP evaporation channel

Isospin diffusion: Isospin transport ratio

Isospin transport ratio technique: highlight isospin diff. F. Rami et al., PRL84, 1120 (2000)

Given $A = {}^{64}$Ni, $B = {}^{58}$Ni:

$$R(X) = \frac{2X_i - X_{AA} - X_{BB}}{X_{AA} - X_{BB}}$$

- $R(X) = \pm 1 \rightarrow$ non equilibrated cond.
- $R(X) = 0 \rightarrow$ complete equilibrium

where $i = AA, AB, BA, BB$ and X is an isospin sensitive observable (e.g. $\langle N/Z \rangle_{QPr}$).
$\rightarrow$ bypass effects acting similarly on the four systems (apparatus acceptance or physical processes e.g. statistical decay)

- Both asymmetric "branches" driven towards $R(\langle N/Z \rangle) = 0$ for low p_{red}
- Complete equilibration is not reached $\rightarrow$ central collisions not considered

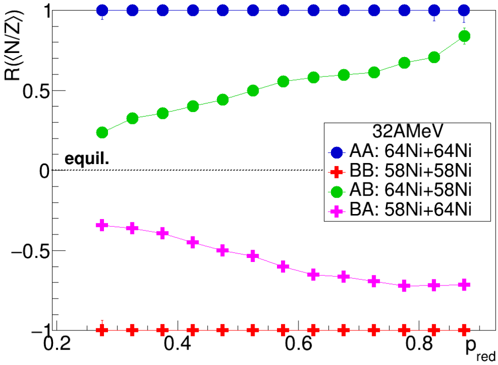

QP evaporation channel

Isospin diffusion: Isospin transport ratio

Isospin transport ratio technique: highlight isospin diff. F. Rami et al., PRL84, 1120 (2000)

Given $A = ^{64}Ni$, $B = ^{58}Ni$:

$$R(X) = \frac{2X_i - X_{AA} - X_{BB}}{X_{AA} - X_{BB}}$$

$R(X) = \pm 1 \rightarrow$ non equilibrated cond.

$R(X) = 0 \rightarrow$ complete equilibrium

where $i = AA, AB, BA, BB$ and X is an isospin sensitive observable (e.g. $\langle N/Z \rangle_{QPr}$).

$\rightarrow$ bypass effects acting similarly on the four systems (apparatus acceptance or physical processes e.g. statistical decay)

- Both asymmetric "branches" driven towards $R(\langle N/Z \rangle) = 0$ for low p_{red}
- Complete equilibration is not reached $\rightarrow$ central collisions not considered
- Comparison 32 $AMeV$ - 52 $AMeV$: *higher degree of equilibration at 32 $AMeV$, as expected due to longer interaction timescale.*

C.Ciampi et al., PRC 106, 024603 (2022)

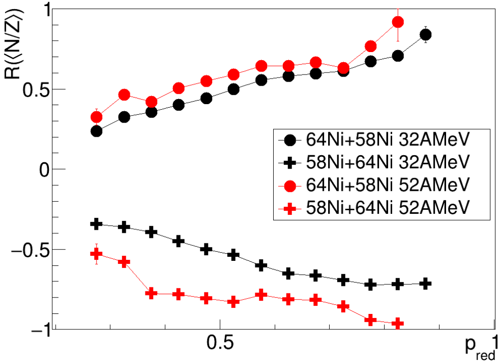

QP evaporation channel

Isospin diffusion: Isospin transport ratio

Isospin transport ratio technique: highlight isospin diff. F. Rami et al., PRL84, 1120 (2000)

Given $A = {}^{64}$Ni, $B = {}^{58}$Ni:

$$R(X) = \frac{2X_i - X_{AA} - X_{BB}}{X_{AA} - X_{BB}}$$

- $R(X) = \pm 1 \rightarrow$ non equilibrated cond.
- $R(X) = 0 \rightarrow$ complete equilibrium

where $i = AA, AB, BA, BB$ and X is an isospin sensitive observable (e.g. $\langle N/Z \rangle_{QPr}$).
$\rightarrow$ bypass effects acting similarly on the four systems (apparatus acceptance or physical processes e.g. statistical decay)

- Both asymmetric "branches" driven towards $R(\langle N/Z \rangle) = 0$ for low p_{red}
- Complete equilibration is not reached $\rightarrow$ central collisions not considered
- Comparison 32 AMeV - 52 AMeV: *higher degree of equilibration at 32 AMeV, as expected due to longer interaction timescale.*
  C.Ciampi et al., PRC 106, 024603 (2022)

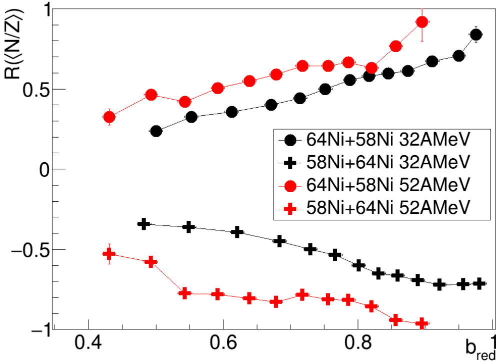

QP breakup channel (QPb)

QP breakup channel
QPb channel selection

QP breakup: events with $\mathbf{M_{big} = 2}$.
Both fragments must come from QP.

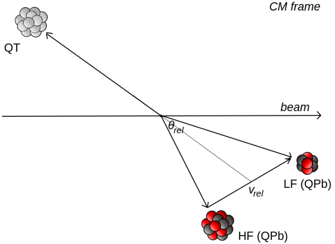

QP breakup channel

QPb channel selection

QP breakup: events with $\mathbf{M_{big} = 2}$. Both fragments must come from QP.

Correlation θ_{rel} vs v_{rel} of the two fragments $Z \geq 5$:

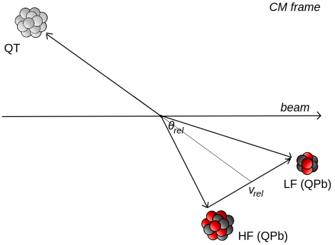

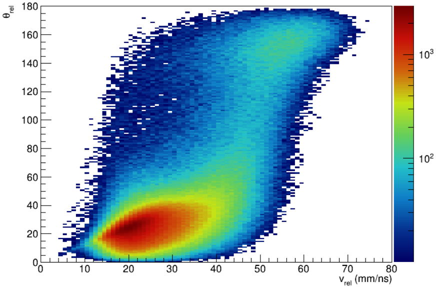

QP breakup: events with $\mathbf{M_{big} = 2}$.
Both fragments must come from QP.

Correlation θ_{rel} vs v_{rel} of the two fragments $Z \geq 5$:

- $\theta_{rel} > 120°$: QP+QT (fragment)

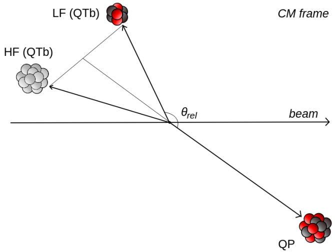

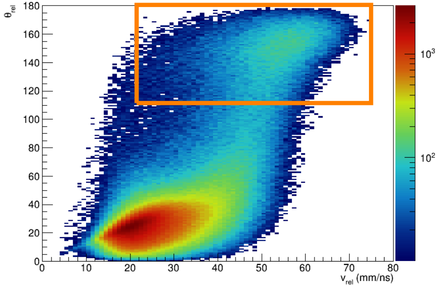

QP breakup channel

QPb channel selection

QP breakup: events with $\mathbf{M_{big} = 2}$.
Both fragments must come from QP.

Correlation θ_{rel} vs v_{rel} of the two fragments $Z \geq 5$:

- $\theta_{rel} > 120°$: QP+QT (fragment)
- $\theta_{rel} < 90°$: QP breakup, both HF and LF detected.

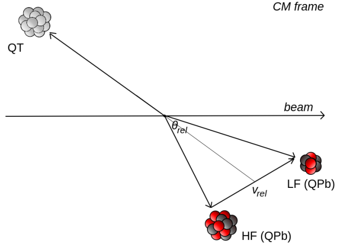

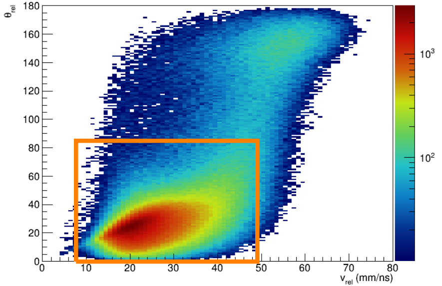

QP breakup channel

QPb channel selection

QP breakup: events with $\mathbf{M_{big} = 2}$.
Both fragments must come from QP.

Correlation θ_{rel} vs v_{rel} of the two fragments $Z \geq 5$:

- $\theta_{rel} > 120°$: QP+QT (fragment)
- $\theta_{rel} < 90°$: QP breakup, both HF and LF detected.

Conditions also on the v_{rel} depending on the reaction energy, and on $Z_H + Z_L \geq 15$.

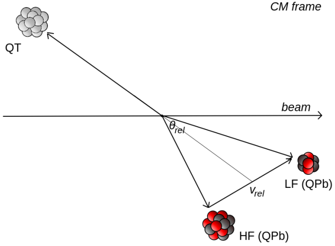

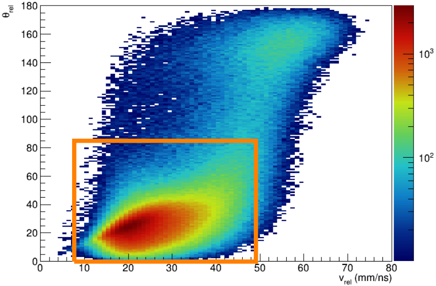

QP breakup channel

Selected events

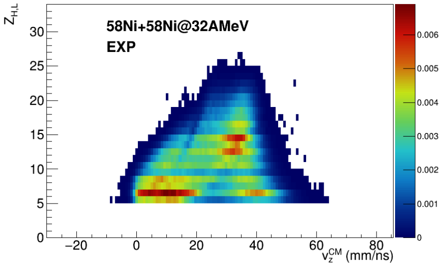

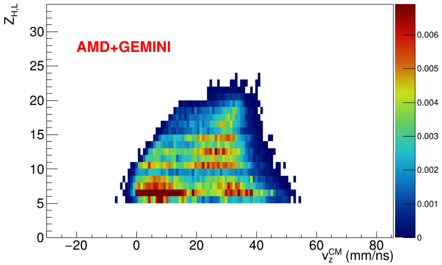

QP breakup channel

Selected events

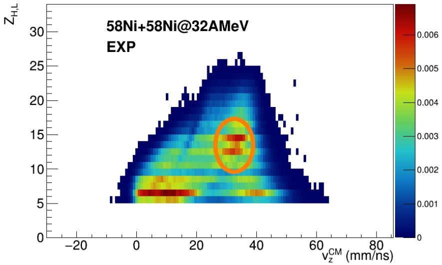

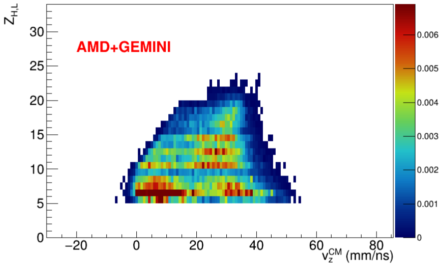

QP breakup channel

Selected events

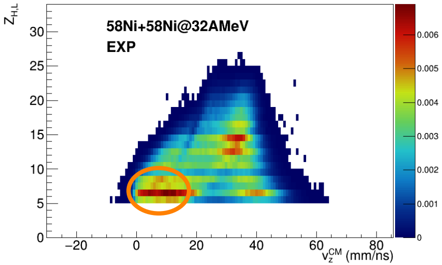

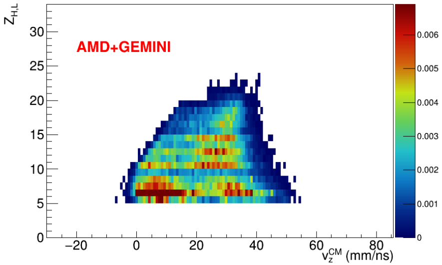

QP breakup channel

Selected events

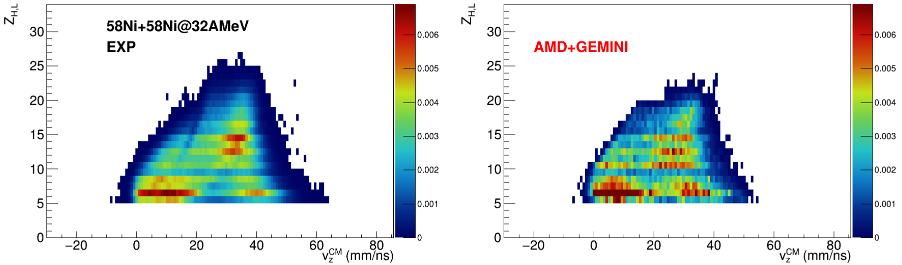

We reconstruct the QP from HF and LF: $Z_{rec} = Z_H + Z_L$ and v_{rec} of their CM.

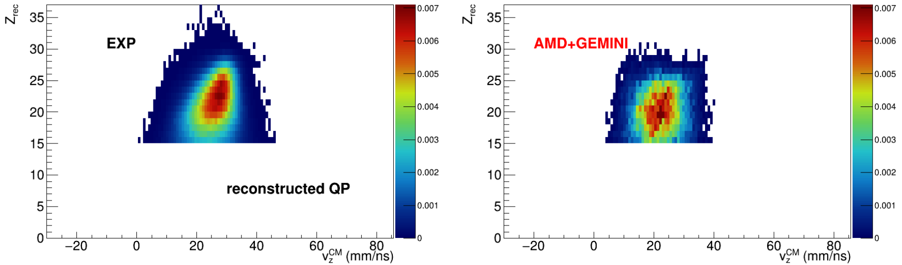

QP breakup channel

Selected events

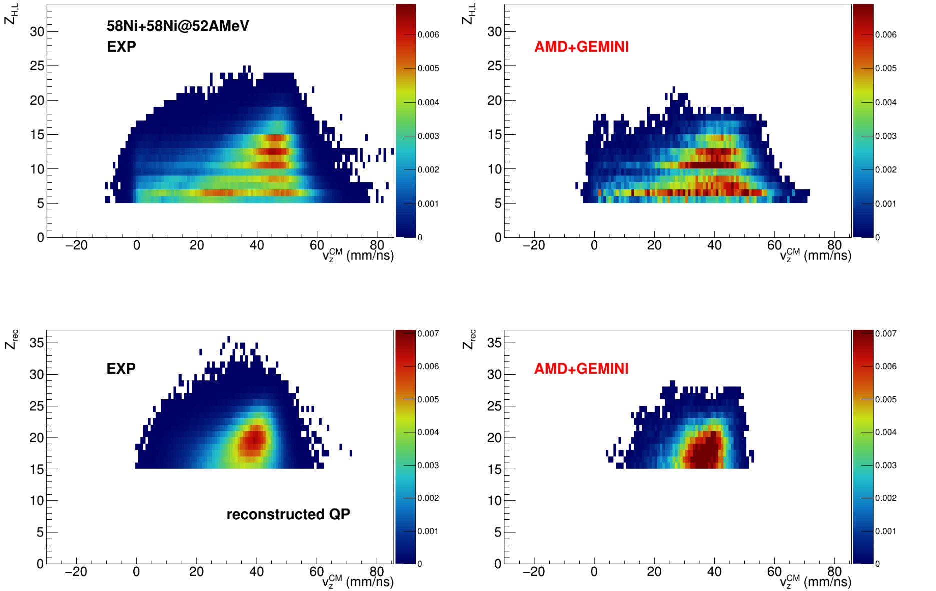

QP breakup channel

Characteristics of the breakup fragments

Charge asymmetry between H and L:

$$\eta = \frac{Z_H - Z_L}{Z_{rec}}$$

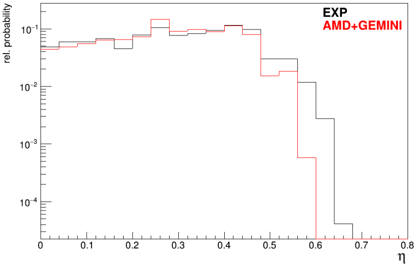

QP breakup channel

Characteristics of the breakup fragments

Charge asymmetry between H and L:

$$\eta = \frac{Z_H - Z_L}{Z_{rec}}$$

- three η intervals:
  - (a) $\eta \leq 0.2 \rightarrow$ symmetric
  - (b) $0.2 < \eta \leq 0.4$
  - (c) $0.4 < \eta \leq 0.6 \rightarrow$ asymmetric

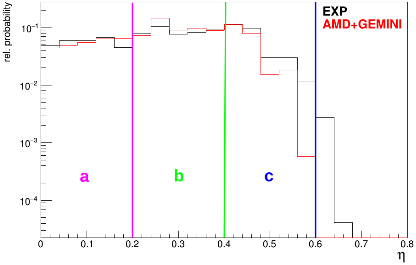

QP breakup channel

Characteristics of the breakup fragments

Charge asymmetry between H and L:

$$\eta = \frac{Z_H - Z_L}{Z_{rec}}$$

- three η intervals:
  - (a) $\eta \leq 0.2 \rightarrow$ symmetric
  - (b) $0.2 < \eta \leq 0.4$
  - (c) $0.4 < \eta \leq 0.6 \rightarrow$ asymmetric

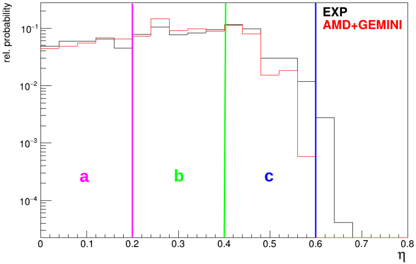

α angle between the QP-QT separation axis ($\vec{v}_{QP_{rec}}$) and the breakup axis ($\vec{v}_{rel}$):

- in the asymmetric configuration the backward emission of the LF is favoured, as expected

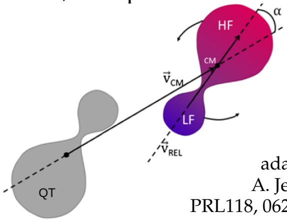

adapted from A. Jedele et al., PRL118, 062501 (2017)

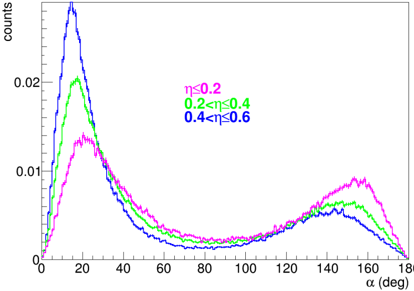

QP breakup channel

Isospin diffusion: $\langle N/Z \rangle$ of the reconstructed QP

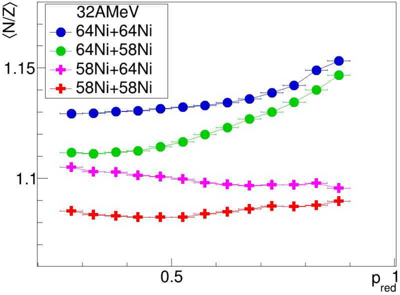

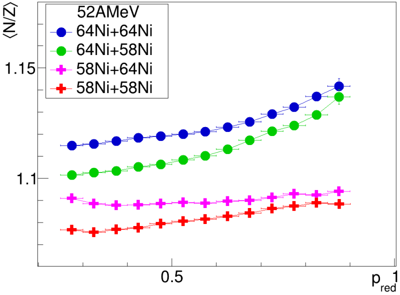

The isospin equilibration is clearly visible also from the characteristics of the QP reconstructed from the two breakup fragments in the QPb channel.
→ **evidence of isospin diffusion**

QP breakup channel

Isospin diffusion: $\langle N/Z \rangle$ of the reconstructed QP

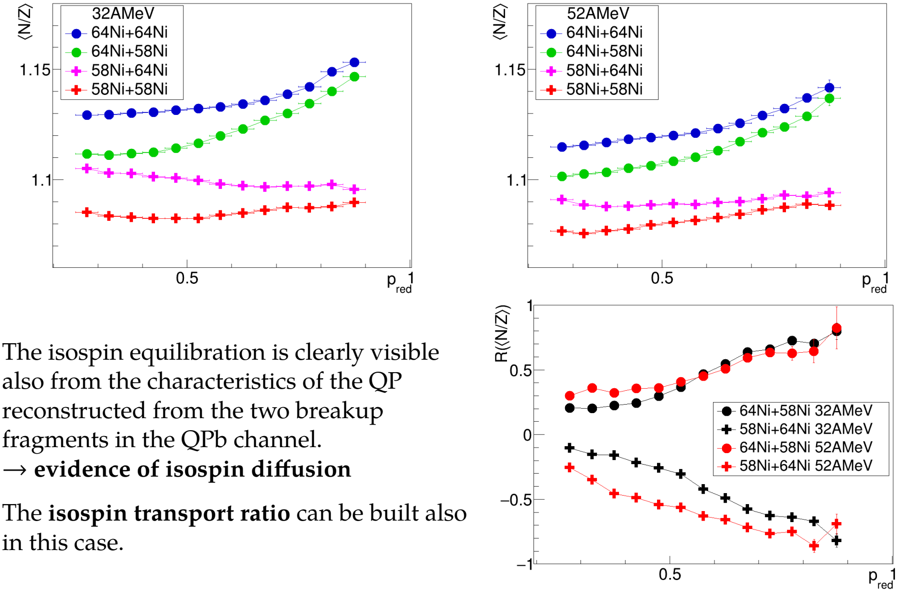

The isospin equilibration is clearly visible also from the characteristics of the QP reconstructed from the two breakup fragments in the QPb channel.
→ **evidence of isospin diffusion**

The **isospin transport ratio** can be built also in this case.

Isospin diffusion

Comparison between the QPr and QPb channels

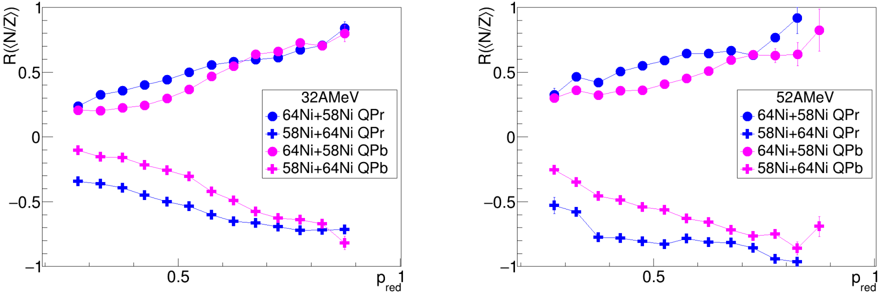

Compare the isospin equilibration in the two reaction channels:

- At both energies, for the same p_{red} value ($\Rightarrow$ same reaction centrality) a higher degree of isospin equilibration is obtained in the QPb channel than in the QPr channel.

Isospin diffusion

Comparison between the QPr and QPb channels

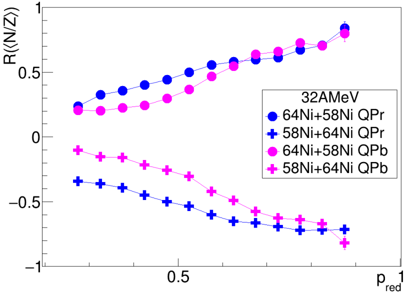

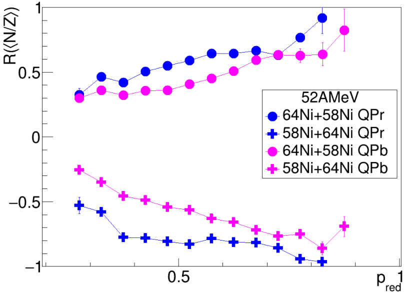

Compare the isospin equilibration in the two reaction channels:

- At both energies, for the same p_{red} value ($\Rightarrow$ same reaction centrality) a higher degree of isospin equilibration is obtained in the QPb channel than in the QPr channel.
- Slight difference in the p_{red} vs b_{red} correlation

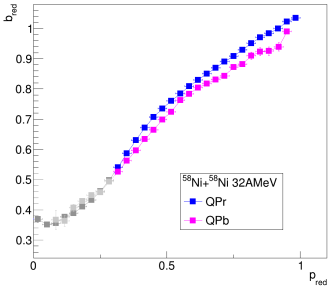

Isospin diffusion

Comparison between the QPr and QPb channels

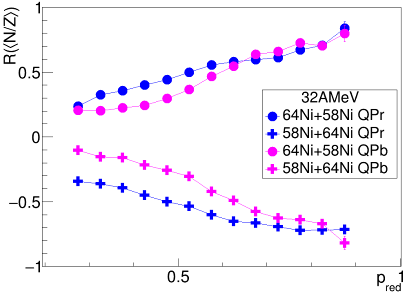

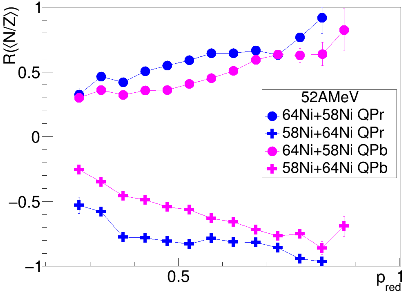

Compare the isospin equilibration in the two reaction channels:

- At both energies, for the same p_{red} value ($\Rightarrow$ same reaction centrality) a higher degree of isospin equilibration is obtained in the QPb channel than in the QPr channel.
- Slight difference in the p_{red} vs b_{red} correlation

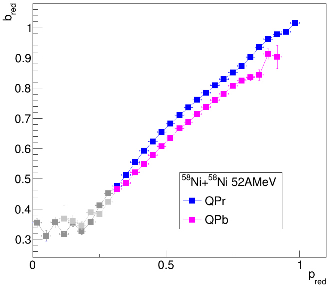

Isospin diffusion

Comparison between the QPr and QPb channels

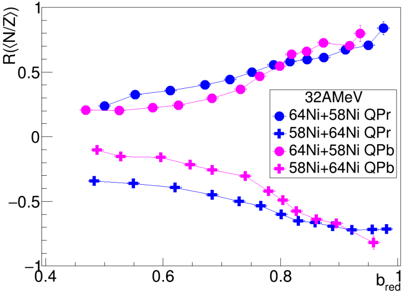

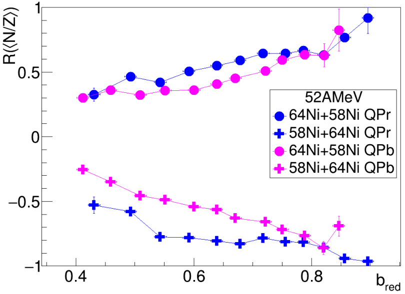

Compare the isospin equilibration in the two reaction channels:

- At both energies, for the same p_{red} value ($\Rightarrow$ same reaction centrality) a higher degree of isospin equilibration is obtained in the QPb channel than in the QPr channel.
- Slight difference in the p_{red} vs b_{red} correlation $\rightarrow$ same result after x-axis rescaling from p_{red} to b_{red}

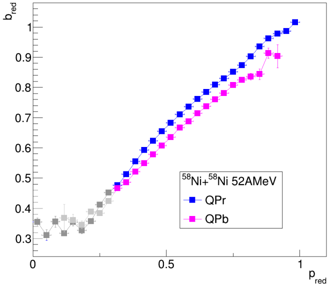

Summary and future perspectives

Summary:

- INDRA-FAZIA E789: ^{64,58}Ni+^{64,58}Ni at 32 AMeV and 52 AMeV
- Selection of QP evaporation (QPr) and QP breakup (QPb) channels
- QP-QT isospin equilibration in the two reaction channels:

Summary and future perspectives

Summary:

- INDRA-FAZIA E789: ^{64,58}Ni+^{64,58}Ni at 32 *A*MeV and 52 *A*MeV
- Selection of QP evaporation (QPr) and QP breakup (QPb) channels
- QP-QT isospin equilibration in the two reaction channels:
  - stronger equilibration at lower beam energy

Summary and future perspectives

Summary:

- INDRA-FAZIA E789: ^{64,58}Ni+^{64,58}Ni at 32 AMeV and 52 AMeV
- Selection of QP evaporation (QPr) and QP breakup (QPb) channels
- QP-QT isospin equilibration in the two reaction channels:
  - stronger equilibration at lower beam energy
  - stronger equilibration in QPb channel than in QPr channel

Summary and future perspectives

Summary:

- INDRA-FAZIA E789: ^{64,58}Ni+^{64,58}Ni at 32 AMeV and 52 AMeV
- Selection of QP evaporation (QPr) and QP breakup (QPb) channels
- QP-QT isospin equilibration in the two reaction channels:
  - stronger equilibration at lower beam energy
  - stronger equilibration in QPb channel than in QPr channel
- Isospin analysis also for other kinds of products:
  - QP breakup fragments HF and LF: their equilibration is compatible with picture proposed in literature
  - LCPs and IMFs: both isospin diffusion and drift hints

Summary and future perspectives

Summary:

- INDRA-FAZIA E789: ^{64,58}Ni+^{64,58}Ni at 32 AMeV and 52 AMeV
- Selection of QP evaporation (QPr) and QP breakup (QPb) channels
- QP-QT isospin equilibration in the two reaction channels:
  - stronger equilibration at lower beam energy
  - stronger equilibration in QPb channel than in QPr channel
- Isospin analysis also for other kinds of products:
  - QP breakup fragments HF and LF: their equilibration is compatible with picture proposed in literature
  - LCPs and IMFs: both isospin diffusion and drift hints

Future perspectives:

- Investigation on the origin of the stronger tendency to isospin equilibration on the reconstructed QP in the breakup channel

Summary and future perspectives

Summary:

- INDRA-FAZIA E789: ^{64,58}Ni+^{64,58}Ni at 32 AMeV and 52 AMeV
- Selection of QP evaporation (QPr) and QP breakup (QPb) channels
- QP-QT isospin equilibration in the two reaction channels:
  - stronger equilibration at lower beam energy
  - stronger equilibration in QPb channel than in QPr channel
- Isospin analysis also for other kinds of products:
  - QP breakup fragments HF and LF: their equilibration is compatible with picture proposed in literature
  - LCPs and IMFs: both isospin diffusion and drift hints

Future perspectives:

- Investigation on the origin of the stronger tendency to isospin equilibration on the reconstructed QP in the breakup channel
- Detailed comparison between experimental data and model predictions, to obtain information on the symmetry energy term of the NEoS
  - Comparison of different models

Summary and future perspectives

Summary:

- INDRA-FAZIA E789: ^{64,58}Ni+^{64,58}Ni at 32 AMeV and 52 AMeV
- Selection of QP evaporation (QPr) and QP breakup (QPb) channels
- QP-QT isospin equilibration in the two reaction channels:
  - stronger equilibration at lower beam energy
  - stronger equilibration in QPb channel than in QPr channel
- Isospin analysis also for other kinds of products:
  - QP breakup fragments HF and LF: their equilibration is compatible with picture proposed in literature
  - LCPs and IMFs: both isospin diffusion and drift hints

Future perspectives:

- Investigation on the origin of the stronger tendency to isospin equilibration on the reconstructed QP in the breakup channel
- Detailed comparison between experimental data and model predictions, to obtain information on the symmetry energy term of the NEoS
  - Comparison of different models
- Stay tuned for the upcoming INDRA-FAZIA experiments!
  - New read-out electronics for INDRA, allowing for better isotopic identification

Thank you

Backup slides

QP evaporation channel

Characteristics of the QP remnant

QP remnant charge distribution

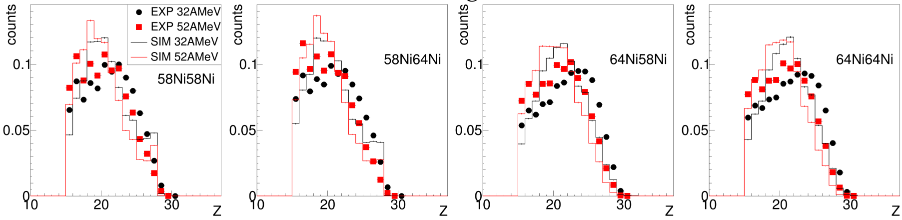

QP remnant velocity distribution

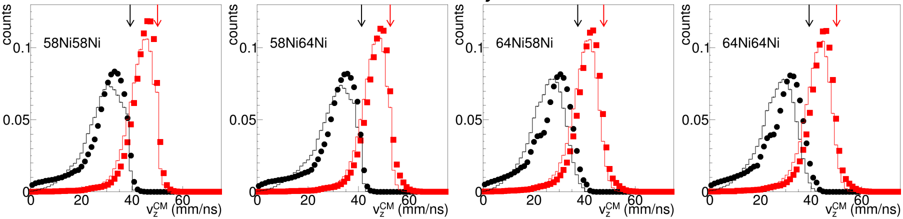

QP breakup channel

Characteristics of the reconstructed QP

Reconstructed QP charge distribution

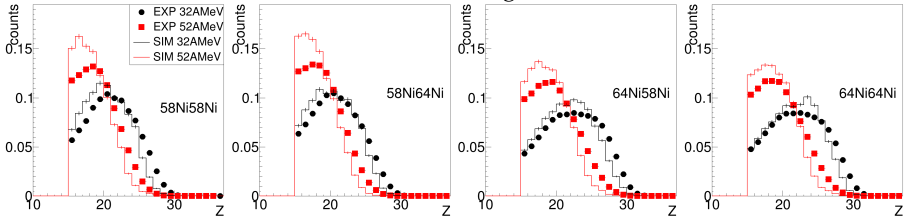

Reconstructed QP velocity distribution

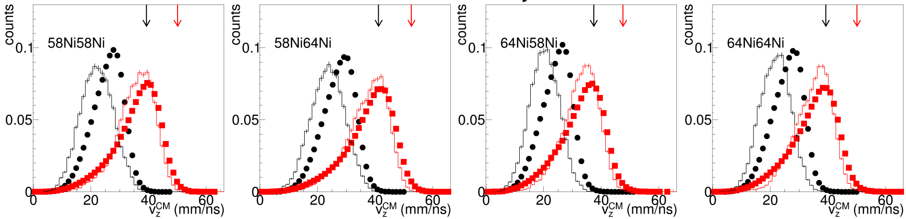

Breakup of the QP
What are we looking for?

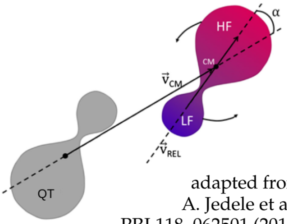

adapted from
A. Jedele et al.,
PRL118, 062501 (2017)

- For a longer time interval elapsed between the QP-QT split and the QP breakup:
    - the α angle between the separation axis $\hat{v}_{CM}$ and the breakup axis $\hat{v}_{rel}$ increases: if the breakup timescale is short compared to the QP rotation period, α can be adopted as a "clock"
    - the degree of isospin equilibration inside the original QP increases → neutron content of the breakup fragments HF and LF

- Within this interpretation of the phenomenon:
    - small α angle → limited isospin equilibration HF-LF (LF similar to neck)
    - large α angle → higher degree of isospin equilibration between HF e LF
- *Equilibration chronometry*: study of isospin observables for HF and LF as a function of α → timescale of isospin equilibration ($\sim$ zs)
- In a recent study, no correlation between the α angle and $(t_{breakup} - t_{DIC})$ has been found in the framework of the dynamical model AMD

Characteristics of the breakup fragments

Isospin equilibration between HF and LF

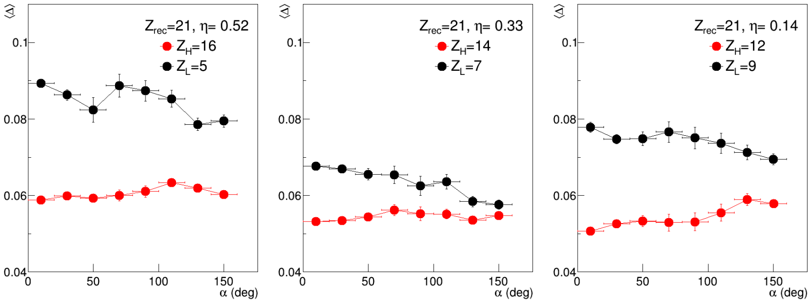

$\langle\Delta\rangle = \langle\frac{N-Z}{A}\rangle$ of the two breakup fragments as a function of the α angle:

- Data trends compatible with the picture proposed in literature:
  - LF more neutron rich than the HF.
  - larger HF-LF asymmetry for low α angles, more equilibrated for increasing α

Characteristics of the breakup fragments

Isospin equilibration between HF and LF

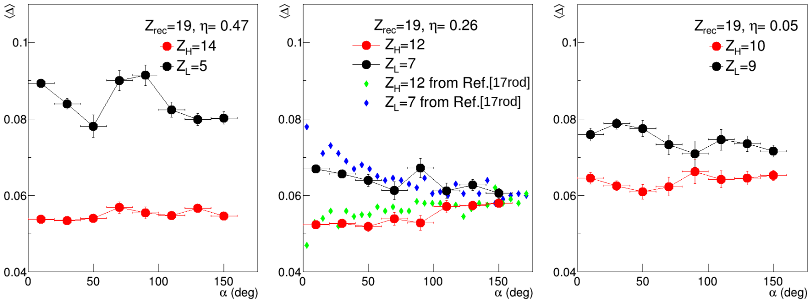

$\langle \Delta \rangle = \langle \frac{N-Z}{A} \rangle$ of the two breakup fragments as a function of the α angle:

- Data trends compatible with the picture proposed in literature:
  - LF more neutron rich than the HF.
  - larger HF-LF asymmetry for low α angles, more equilibrated for increasing α
- Within the small charge asymmetries explored, $\langle \Delta \rangle_L$ depends mostly on the identity of the LF, and less on the partner HF
- Results for $Z_H = 12, Z_L = 7$ are quite comparable to A. Rodriguez Manso et al., PRC95, 044604 (2017)

Isospin drift

QPr channel: LCPs and IMFs

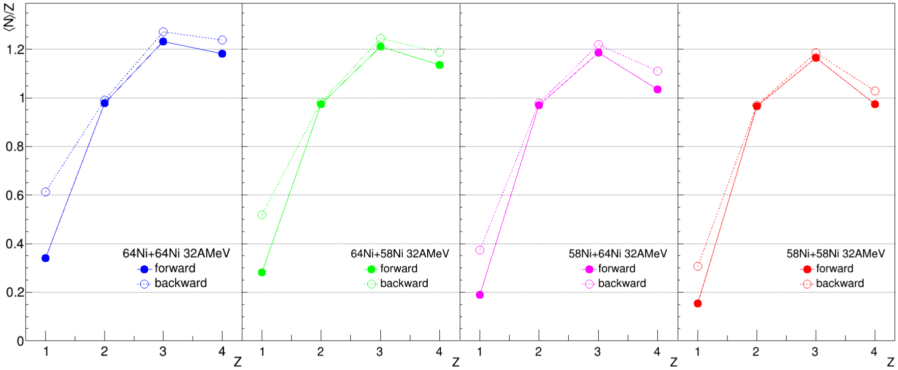

- We analyse the isospin content of LCPs and IMFs according to their emission pattern, i.e. their orientation with respect to the QP remnant:
  - forward: forward QPr emission of LCPs and IMFs
  - backward: backward QPr emission of LCPs and IMFs, with $v_z^{CM} > 0$
- **Isospin drift** $\rightarrow \langle N \rangle$ for the backward emissions is higher than the forward one. Clean interpretation for symmetric systems.

Isospin drift

QPr channel: LCPs and IMFs

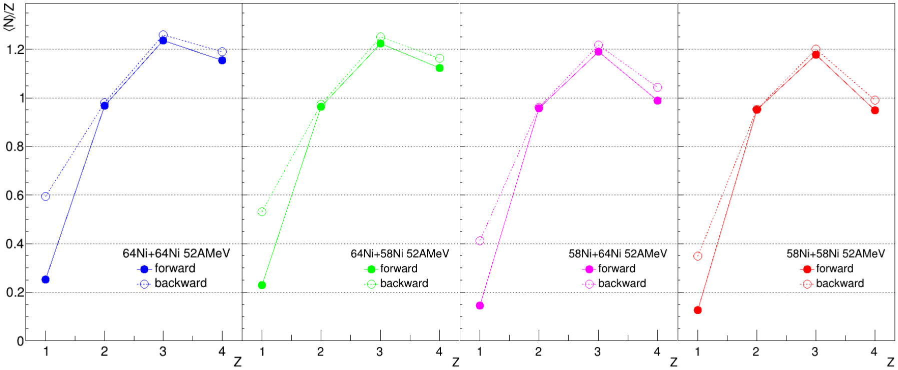

- We analyse the isospin content of LCPs and IMFs according to their emission pattern, i.e. their orientation with respect to the QP remnant:
    - forward: forward QPr emission of LCPs and IMFs
    - backward: backward QPr emission of LCPs and IMFs, with $v_z^{CM} > 0$
- **Isospin drift** $\rightarrow \langle N \rangle$ for the backward emissions is higher than the forward one. Clean interpretation for symmetric systems.

Isospin diffusion

QPr channel: characteristics of the evaporated particles (I)

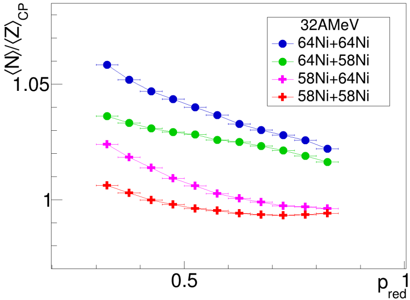

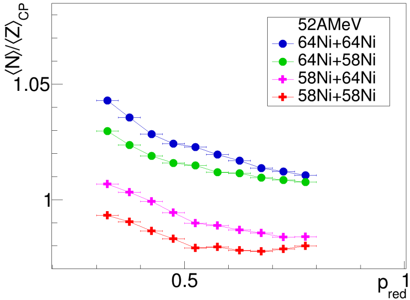

The QP-QT isospin equilibration can be evidenced also on the characteristics of the QP deexcitation emissions.

→ e.g., isospin ratio for complex particles forward emitted with respect to the QP remnant.

$$\langle N\rangle/\langle Z\rangle_{CP} = \sum_i \sum_\nu N_\nu^i / \sum_i \sum_\nu Z_\nu^i$$

considering LCPs and IMFs with $A > 1$.

see E. Galichet et al., PRC 79, 064614 (2009)

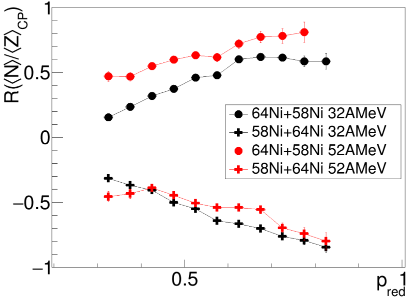

Isospin diffusion

QPr channel: characteristics of the evaporated particles (I)

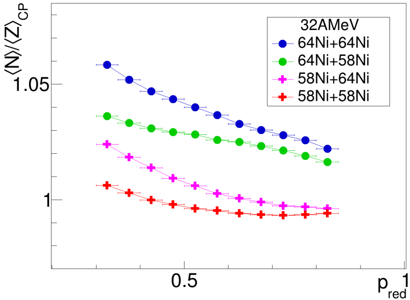

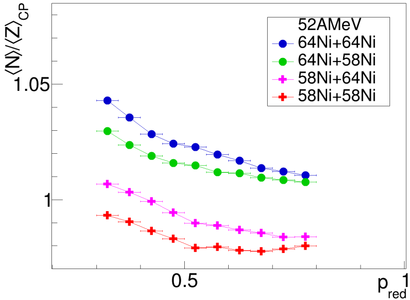

The QP-QT isospin equilibration can be evidenced also on the characteristics of the QP deexcitation emissions.
→ e.g., isospin ratio for complex particles forward emitted with respect to the QP remnant.

$$\langle N\rangle/\langle Z\rangle_{CP} = \sum_i \sum_\nu N^i_\nu / \sum_i \sum_\nu Z^i_\nu$$

considering LCPs and IMFs with $A > 1$.

see E. Galichet et al., PRC 79, 064614 (2009)

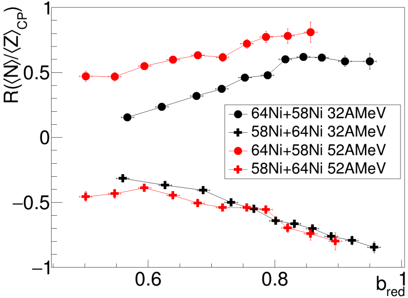

Isospin diffusion

QPr channel: characteristics of the evaporated particles (II)

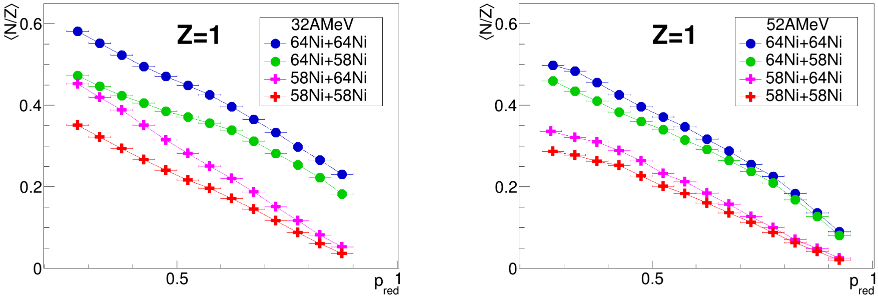

We can consider, e.g., $Z = 1$ particles forward emitted with respect to the QP remnant.

Isospin diffusion

QPr channel: characteristics of the evaporated particles (II)

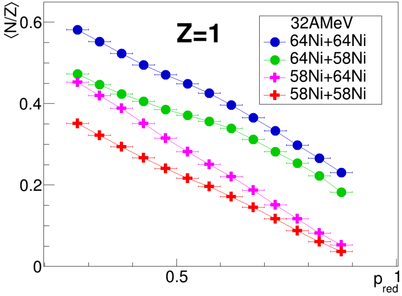

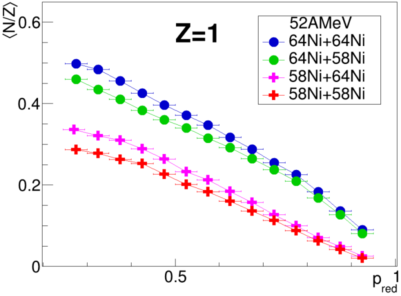

We can consider, e.g., $Z = 1$ particles forward emitted with respect to the QP remnant.

We build the **isospin transport ratio**. The higher degree of equilibration at 32 *A*MeV is confirmed.

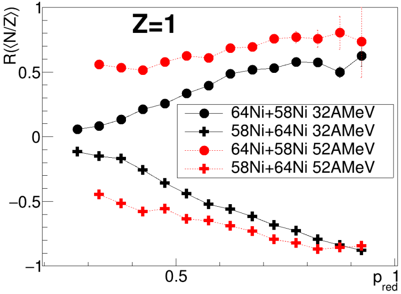

Isospin diffusion

Comparison between the QPr and QPb channels: model predictions

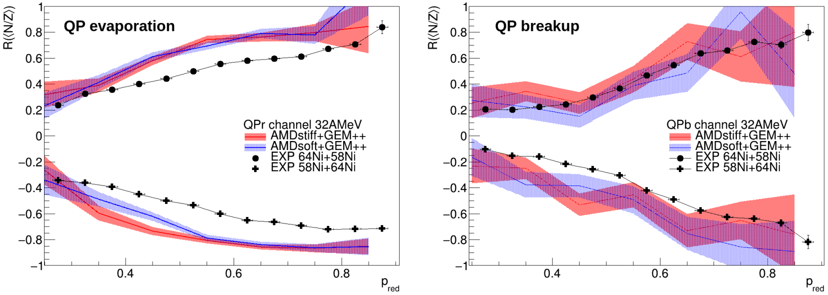

Comparison with model predictions:

- No sensitivity to the parametrisation of the E_{sym} of the NEoS

Isospin diffusion

Comparison between the QPr and QPb channels: model predictions

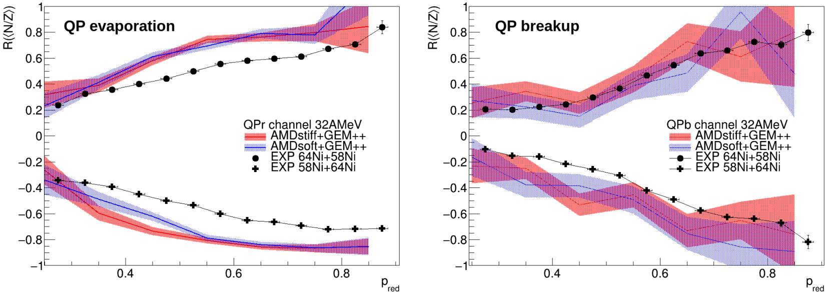

Comparison with model predictions:

- No sensitivity to the parametrisation of the E_{sym} of the NEoS
- Clear evolution towards isospin equilibration in the model:
  - QPr: generally lower degree of equilibration in simulated data
  - QPb: larger error bars in the model (low statistics), but rather good agreement with experimental data

Isospin diffusion

Comparison between the QPr and QPb channels: model predictions

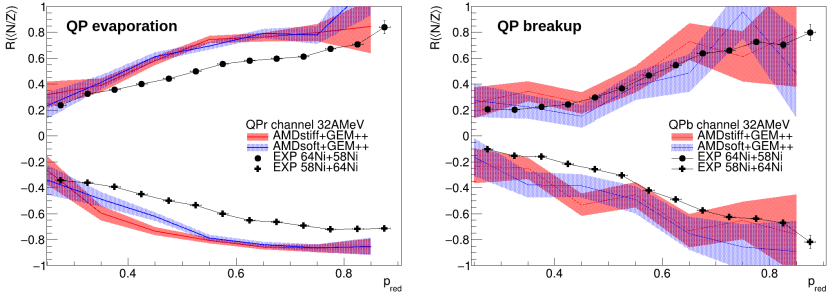

Comparison with model predictions:

- No sensitivity to the parametrisation of the E_{sym} of the NEoS
- Clear evolution towards isospin equilibration in the model:
  - QPr: generally lower degree of equilibration in simulated data
  - QPb: larger error bars in the model (low statistics), but rather good agreement with experimental data
- Simulated data confirm the stronger tendency to isospin equilibration in QPb channel than in QPr channel

Isospin diffusion

Comparison between the QPr and QPb channels: model predictions

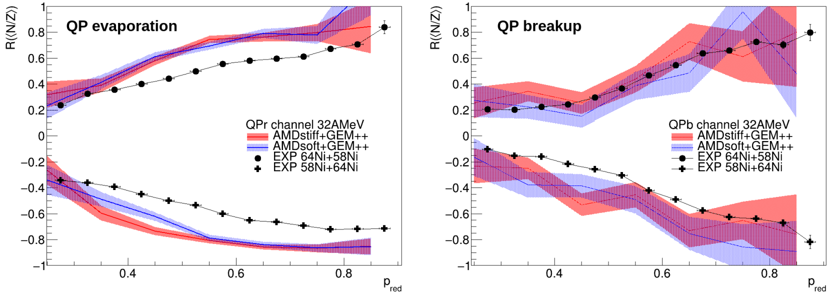

Comparison with model predictions:

- No sensitivity to the parametrisation of the E_{sym} of the NEoS
- Clear evolution towards isospin equilibration in the model:
  - QPr: generally lower degree of equilibration in simulated data
  - QPb: larger error bars in the model (low statistics), but rather good agreement with experimental data
- Simulated data confirm the stronger tendency to isospin equilibration in QPb channel than in QPr channel → investigate the difference

Experimental setup

Identification techniques

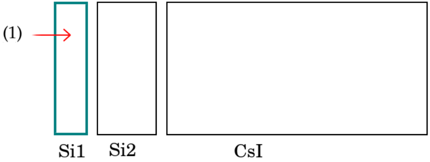

Different identification methods depending on the stopping layer:

1. Si1: PSA-Si

Pulse Shape Analysis: identification of fragments stopped in a detector (e.g. Si1)

Signal shape ← Ionisation density ← (Z, A) and E of fragment

Experimental setup

Identification techniques

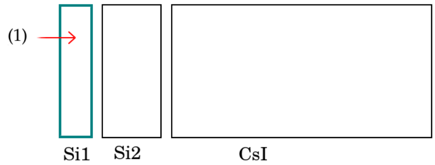

Different identification methods depending on the stopping layer:

1. Si1: PSA-Si

Pulse Shape Analysis: identification of fragments stopped in a detector (e.g. Si1)

Signal shape ← Ionisation density ← (Z, A) and E of fragment

Signal shape → Shape-related parameter → PSAq: E vs t_{rise} ; PSAi: E vs I_{max}

- A good doping uniformity is mandatory
- Si detectors are reverse mounted

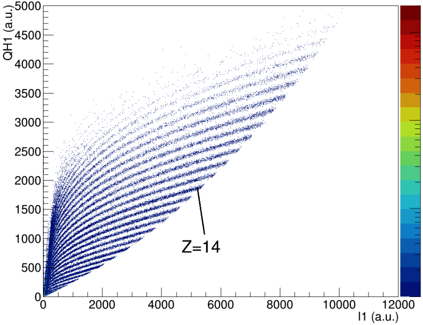

Experimental setup

Identification techniques

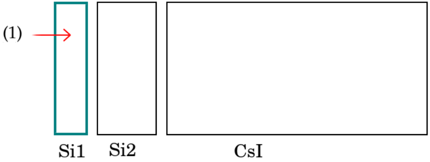

Different identification methods depending on the stopping layer:

1. Si1: PSA-Si

Pulse Shape Analysis: identification of fragments stopped in a detector (e.g. Si1)

Signal shape ← Ionisation density ← (Z, A) and E of fragment

Signal shape → Shape-related parameter → PSAq: E vs t_{rise} / PSAi: E vs I_{max}

- A good doping uniformity is mandatory
- Si detectors are reverse mounted

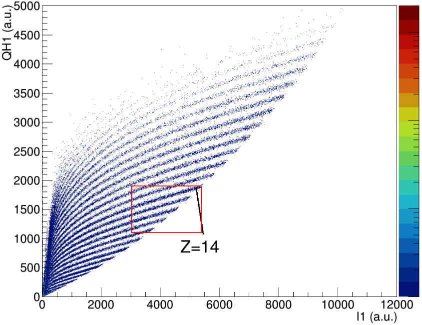

Experimental setup

Identification techniques

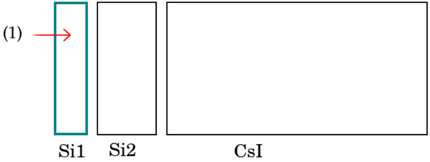

Different identification methods depending on the stopping layer:

1. Si1: PSA-Si

Pulse Shape Analysis: identification of fragments stopped in a detector (e.g. Si1)

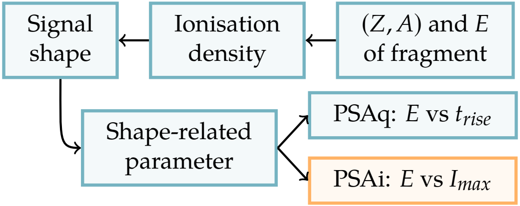

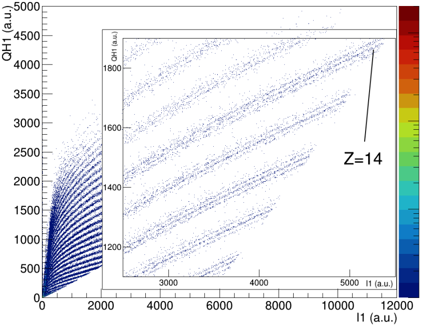

- A good doping uniformity is mandatory
- Si detectors are reverse mounted

Experimental setup

Identification techniques

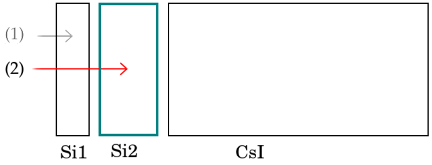

Different identification methods depending on the stopping layer:

1. Si1: PSA-Si
2. Si2: ΔE-E Si1-Si2

ΔE-E technique: based on the mechanism of kinetic energy dissipation of charged particles in matter $\rightarrow$ Bethe-Bloch

$$-\frac{dE}{dx} = \frac{4\pi e^4 Z^2}{m_e v^2} Nz \left[\ln \frac{2m_e v^2}{I} - \ln(1-\beta^2) - \beta^2 \right]$$

In a non-relativistic approx. ($E_0 = \Delta E + E_{res}$):

$$\Delta E \propto \frac{Z^2}{v^2} \cdot \Delta x \propto \frac{Z^2 A}{E_0} \cdot \Delta x \Rightarrow \Delta E \cdot E_0 = kZ^2 A$$

Identify the ejectiles stopped in the second stage detector

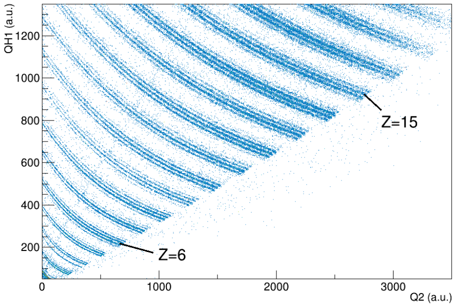

Experimental setup

Identification techniques

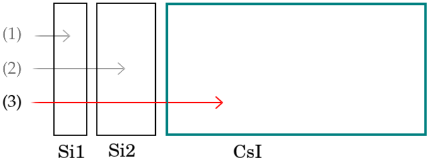

Different identification methods depending on the stopping layer:

1. Si1: PSA-Si
2. Si2: ΔE-E Si1-Si2
3. CsI: ΔE-E Si2-CsI

Δ***E-E technique***: based on the mechanism of kinetic energy dissipation of charged particles in matter → Bethe-Bloch

$$-\frac{dE}{dx} = \frac{4\pi e^4 Z^2}{m_e v^2} Nz \left[\ln \frac{2m_e v^2}{I} - \ln(1-\beta^2) - \beta^2 \right]$$

In a non-relativistic approx. ($E_0 = \Delta E + E_{res}$):

$$\Delta E \propto \frac{Z^2}{v^2} \cdot \Delta x \propto \frac{Z^2 A}{E_0} \cdot \Delta x \Rightarrow \Delta E \cdot E_0 = kZ^2 A$$

Identify the ejectiles stopped in the second stage detector, and also in the third stage

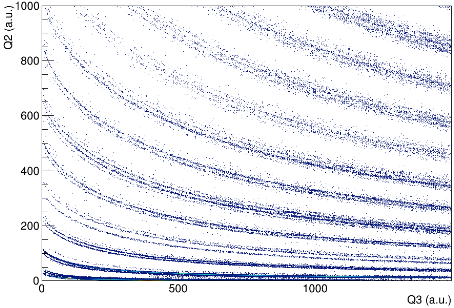

Experimental setup

Identification techniques

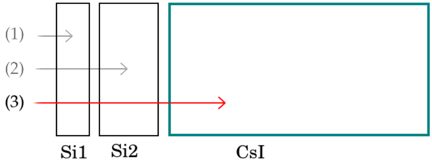

Different identification methods depending on the stopping layer:

1. Si1: PSA-Si
2. Si2: ΔE-E Si1-Si2
3. CsI: ΔE-E Si2-CsI or PSA-CsI

Pulse Shape Analysis in CsI: used for high-energy LCPs.
Intensity of scintillation light:

$$I(t) = I_{fast} \cdot \frac{e^{-t/\tau_{fast}}}{\tau_{fast}} + I_{slow} \cdot \frac{e^{-t/\tau_{slow}}}{\tau_{slow}}$$

where $\tau_{fast} \sim 700\,\text{ns}$ and $\tau_{slow} \sim 5\,\mu\text{s}$. The ratio I_{fast}/I_{slow} depends on (Z, A) and E of fragment.
Digital electronics: two trapezoidal shapers with different flat top applied to CsI signal.

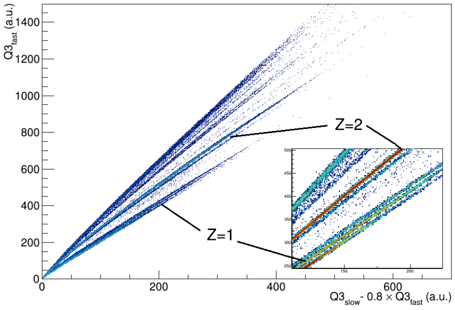

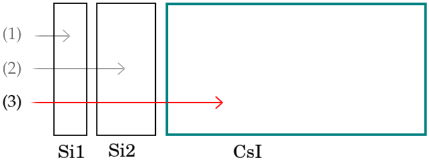

Different identification methods depending on the stopping layer:

1. Si1: PSA-Si
2. Si2: ΔE-E Si1-Si2
3. CsI: ΔE-E Si2-CsI or PSA-CsI

Pulse Shape Analysis in CsI: used for high-energy LCPs.
Intensity of scintillation light:

$$I(t) = I_{fast} \cdot \frac{e^{-t/\tau_{fast}}}{\tau_{fast}} + I_{slow} \cdot \frac{e^{-t/\tau_{slow}}}{\tau_{slow}}$$

where $\tau_{fast} \sim 700\,\text{ns}$ and $\tau_{slow} \sim 5\,\mu\text{s}$. The ratio I_{fast}/I_{slow} depends on (Z, A) and E of fragment.
Digital electronics: two trapezoidal shapers with different flat top applied to CsI signal.